Surface Observed Global Land Precipitation Variations during 1900–88

AIGUO DAI*

Department of Applied Physics, Columbia University, New York, New York

INEZ Y. FUNG

School of Earth and Ocean Sciences, University of Victoria, Victoria, Canada, and NASA/Goddard Institute for Space Studies, New York, New York

ANTHONY D. DEL GENIO

NASA/Goddard Institute for Space Studies, New York, New York

(Manuscript received 9 July 1996, in final form 11 October 1996)

ABSTRACT

The authors have analyzed global station data and created a gridded dataset of monthly precipitation for the period of 1900–88. Statistical analyses suggest that discontinuities associated with instrumental errors are large for many high-latitude station records, although they are unlikely to be significant for the majority of the stations. The first leading EOF in global precipitation fields is an ENSO-related pattern, concentrating mostly in the low latitudes. The second leading EOF depicts a linear increasing trend ($\sim$2.4 mm decade^{-1}) in global precipitation fields during the period of 1900–88. Consistent with the zonal precipitation trends identified in previous analyses, the EOF trend is seen as a long-term increase mostly in North America, mid- to high-latitude Eurasia, Argentina, and Australia. The spatial patterns of the trend EOF and the rate of increase are generally consistent with those of the precipitation changes in increasing CO_2 GCM experiments.

The North Atlantic oscillation (NAO) accounts for $\sim$10% of December–February precipitation variance over North Atlantic surrounding regions. The mode suggests that during high-NAO-index winters, precipitation is above normal in northern ($>$50°N) Europe, the eastern United States, northern Africa, and the Mediterranean, while below-normal precipitation occurs in southern Europe, eastern Canada, and western Greenland.

Wet and dry months of one standard deviation occur at probabilities close to those of a normal distribution in midlatitudes. In the subtropics, the mean interval between two extreme events is longer. The monthly wet and dry events seldom (probability $<$ 5%) last longer than 2 months. ENSO is the single largest cause of global extreme precipitation events. Consistent with the upward trend in global precipitation, globally, the averaged mean interval between two dry months increased by $\sim$28% from 1900–44 to 1945–88. The percentage of wet areas over the United States has more than doubled (from $\sim$12% to $>$24%) since the 1970s, while the percentage of dry areas has decreased by a similar amount since the 1940s. Severe droughts and floods comparable to the 1988 drought and 1993 flood in the Midwest have occurred 2–9 times in each of several other regions of the world during this century.

1. Introduction

Station rain gauge records have been used to estimate the monthly climatology (e.g., Jaeger 1983; Shea 1986; Legates and Willmott 1990) and large-scale variations of precipitation during this century (Bradley et al. 1987; Diaz et al. 1989; Vinnikov et al. 1990). These large-scale analyses of precipitation changes have revealed that during the last 4–5 decades precipitation has increased over northern midlatitudes and most Southern Hemisphere land areas, but has decreased in northern low-latitude land areas. However, these long-term precipitation trends have been interpreted cautiously due to the possible inhomogeneity and the limited spatial coverage of the precipitation station data (Følland et al. 1990, 1992).

It is well known that terrestrial rain gauge records contain various instrumental errors (Sevruk 1982; Legates and Willmott 1990; Groisman et al. 1991; Groisman and Legates 1994). The errors may be grouped into two types: undercatch and inhomogeneity. The undercatch error, which results from wind blowing, wall wetting, evaporation, and splashing, varies from less than 5% in the Tropics to more than 50% near the poles in winter

* Current affiliation: National Center for Atmospheric Research, Boulder, Colorado.

Corresponding author address: Dr. Aiguo Dai, NCAR, P.O. Box 3000, Boulder, CO 80307.
E-mail: adai@ucar.edu

(Legates and Willmott 1990; Groisman et al. 1991; Sevruk 1993; Groisman and Legates 1994). Inhomogeneities in precipitation records, which result from changes in instrumentation, recording practice, and station locations–environment, may cause 4%–40% changes in precipitation records within a few years and are thought to have occurred one to three times over the last 100 yr at many primary observing stations within various mid- and high-latitude Northern Hemisphere countries (Groisman et al. 1991; Karl et al. 1993). Whereas some of the inhomogeneities may result from station relocation (which is not related to the undercatch error), they are more often induced by instumentation changes through the undercatch bias.

While focusing on zonal and hemispheric long-term changes, previous analyses of large-scale precipitation (Bradley et al. 1987; Diaz et al. 1989; Vinnikov et al. 1990; Eischeid et al. 1991) have not provided quantitative estimates of the uncertainties resulting from instrumental errors and incomplete station coverage. Using a gridding radius of 400 to 500 km and a grid of ~400-km resolution in these studies is physically inappropriate since precipitation has a spatial correlation distance of about half this size, as we show below. Groisman and Easterling (1994) attempted to correct the undercatch bias in North American precipitation (including snowfall) based on metadata and a selection of the ''best'' network and reliable ''first-guess'' estimates, so that the inhomogeneities induced by changes in instrumentation through the undercatch bias could be corrected. Although the correction of the undercatch bias, which itself has large uncertainties and requires a large amount of local meteorological and instrumental data which are not readily available for most stations of global datasets, is certainly an important step forward, other methods are needed for adjusting inhomogeneities that are not related to the undercatch (e.g., due to station relocation).

This study was also motivated by the need to create a well-checked global (land) monthly precipitation dataset for the last 100 yr or so, which is needed in many other global change studies [e.g., in estimating climate effects on atmosphere–biosphere carbon exchanges (Dai and Fung 1993) and interpreting long-term cloudiness trends (Dai et al., 1997)]. Our gridded dataset differs from the ones mentioned above in the following respects. 1) We correct the major discontinuity errors in mid- to high-latitude station records. This makes our dataset more reliable for interpreting climatic signals (e.g., the increasing trend) over these regions. 2) We adopt a gridding radius of 300 km based on the spatial correlation scales of monthly precipitation and the global station distributions, and interpolate only the anomalies onto a 2.5° × 2.5° grid. This should enable our dataset to capture regional patterns more realistically. 3) We present an estimate of spatial sampling errors of the gridded anomalies, which provides a guide for determining whether a regional signal is statistically significant (sampling errors are not discussed in the previous datasets).

In this study, we develop techniques to objectively detect and remove errors induced by instrumental discontinuity (section 3). Our analysis suggests that instrumental discontinuities are large for many high-latitude station records, but globally they are not significant, contrary to previous speculations (Groisman et al. 1991; Karl et al. 1993). We also estimate the uncertainties in derived precipitation changes in large regions due to incomplete station coverage. We compare our derived precipitation changes with other relevant climate changes, such as ENSO cycles and cloudiness changes (section 5), and with previous analyses (section 6). We apply empirical orthogonal function analysis to examine the leading modes of variation in global precipitation anomaly fields over the time period of 1900–88 (section 7). Based on temporal and spatial patterns of the EOFs, we discuss the likely physical processes behind the leading modes of precipitation fields. Since extreme precipitation events such as droughts and floods have the greatest impact on human life and the environment, we also present statistical characteristics of extreme events of precipitation over global land areas (section 8). The precipitation station dataset that we employed is defined in section 2, and the gridding method and sampling errors are presented in section 4. In section 9, we summarize the results.

2. Station precipitation records

The global station dataset of monthly precipitation compiled by Eischeid et al. (1991) was used as the starting point of this study. The dataset includes 5328 stations and contains about 3.8 million records of monthly precipitation for the period of 1900–88. During the compilation, certain quality controls have been imposed (see Eischeid et al. 1991 for details).

The station distribution is illustrated in Fig. 1 for 1900, 1930, 1960, and 1985. Except for a limited number of island stations, there is virtually no coverage over open oceans. Over land, the coverage in the Amazon and central South America, central and northern Asia, the Sahara and the Middle East Deserts, and central Australia has remained poor for most of the time. Figure 2 shows that the number of stations that have 12 monthly records increased steadily from 1850 to 1950 and then stayed at a maximum of ~4000 until about 1970. Thereafter, the number of stations decreased to ~1600 in 1988. According to Vose et al. (1992), the expansion of the network since the late nineteenth century is due to the increased habitation of areas that were previously less populated. The sharp increase in the number of stations in 1951 is due to the inclusion of the 1951–60 version of the World Weather Records (WWR) dataset in the World Monthly Surface Station Climatology. The decrease after 1970 primarily results from the inclusion of only three of the six volumes of the 1971–80 WWR

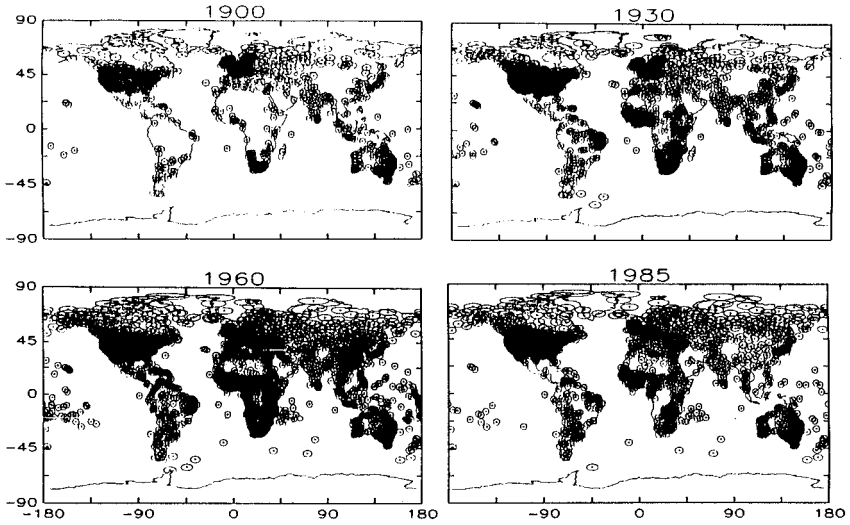

FIG. 1. Global distribution of meteorological stations having at least 6 monthly precipitation records for the indicated years. A circle with a 300-km radius is drawn around each station.

publication (i.e., three volumes have yet to be prepared). The decrease continues through the 1980s because most of the datasets from which the Eischeid et al. (1991) dataset was compiled were produced during the early 1980s or late 1970s. More concerted efforts are needed to compile the station data of the recent decades.

At each station, we computed the monthly precipitation departures from monthly means of the period of 1900–88 and the standard deviations (σ) of the monthly anomalies (outliers outside 5 σ were excluded in computing the mean and the σ using iteration). We rejected station records whose anomalies exceed 5 σ, resulting in an additional elimination of about 2460 monthly records (~0.06% of the total records). Visual inspection of the locations of the stations rejected for selected months did not reveal any spatial coherence associated with meteorological phenomena. These outliers likely resulted from transmission and typographical errors because precipitation histograms suggest many fewer such outliers. In addition, we did not use station records whose length was shorter than 11 yr (~10%).

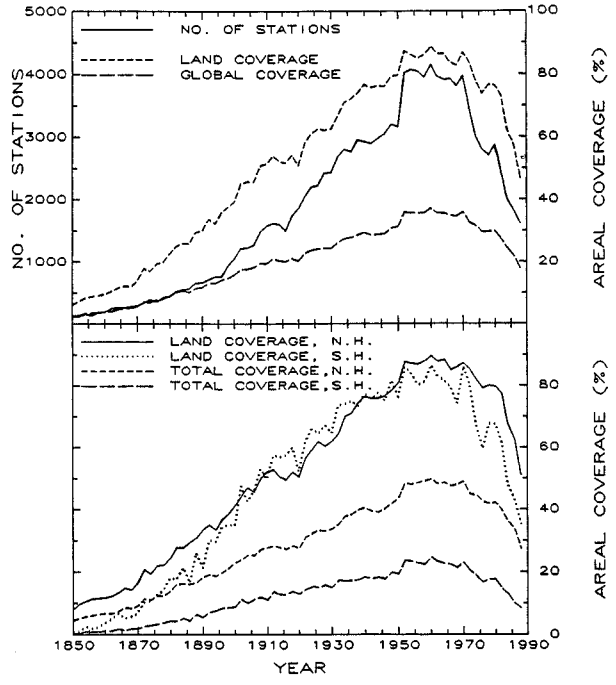

FIG. 2. Upper panel: number of stations having 12 monthly precipitation records (solid line), and the percentages of global land (short broken line) and total (long broken line) areas located within 300 km of a station. Lower panel: hemispheric land and total areas located within 300 km of a station.

We tested different rejection criteria (3 σ, 5 σ, and no rejection) and examined their effects on area-averaged precipitation. The total number of outliers rejected under the 3-σ criterion is about 38 100 or 1%. Since the histograms of monthly precipitation have longer tails on the wet side, the rejected records are almost all positive (wet) anomalies. Although the rejection of $\leq$1% of the records should have negligible effects on station precipitation time series, it can induce bias (underestimates) and spurious long-term changes in large-area-averaged anomalies because the bias is sensitive to station coverage (the lower the station coverage, the larger the bias), which is not constant during this century (cf. Figs. 1 and 2). We find that the 5-σ screening reduces the globe- and hemisphere-integrated anomalies only slightly (~2 mm) compared with the no-screening case (nevertheless, as mentioned above, some gross screening was done during the compilation of the dataset), while the 3-σ screening lowers the integrated anomalies by a significant amount (~20 mm) and induces some long-term changes (~5 mm) as well (Dai 1996). We believe that the 5 σ screening is likely a more appropriate cri-

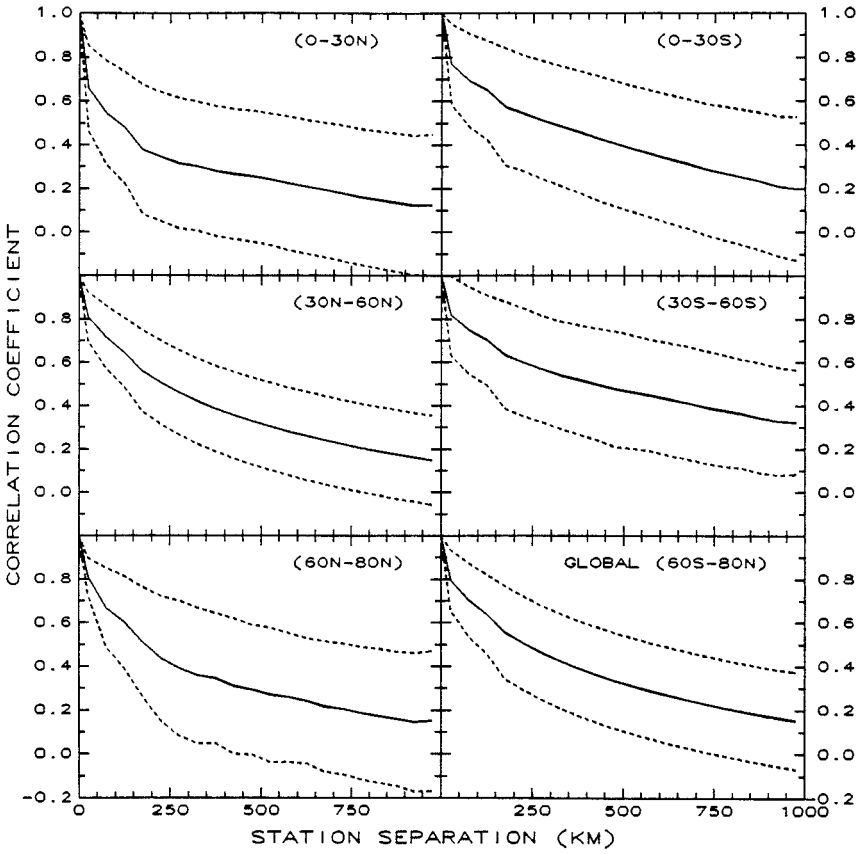

FIG. 3. The mean (solid line) and mean ± one standard deviation limits (dashed lines) of correlation coefficients between annual precipitation anomalies of pairs of stations having at least 30 common yr in their records. The averaging was performed by dividing the separation distance into specified intervals (~50 km) and then averaging all the correlation coefficients within each interval to obtain a mean and standard deviation for the interval.

terion than the 3 σ screening for eliminating transmission and typographic errors, while keeping the artificial bias to a minimum.

We employed an influence radius to represent the size of the surrounding area for which a given station's data may provide significant information on precipitation change. To establish the influence radius, we calculated correlation coefficients between precipitation anomalies of all pairs of stations having at least 30 common years in their records. Both annual and monthly precipitation anomalies were used. Figure 3 shows the correlation coefficients for annual anomalies as a function of station separation (plots for monthly anomalies are similar). As expected, the correlation falls off with separation distance much more rapidly than that of temperature anomalies (Hansen and Lebedeff 1987). The spatial correlation is relatively higher over the Southern Hemisphere than over the Northern Hemisphere, presumably resulting from the orographic and land–sea configuration over the two hemispheres. The effect of sampling length here is likely to be small since there are thousands of station pairs over both the hemispheres. On average, the correlation falls to an insignificant level (≈0.36 for 30-yr-long records) at a separation distance of ~200 km for the zone 0°–30°N, 400 km for 30°–60°N, 300 km for 60°–80°N, 550 km for 0°–30°S, and 800 km for 30°–60°S. Globally, station records of monthly precipitation anomalies are not significantly correlated at separation distances larger than about 450 km.

At 300-km separation, the average correlation coefficient of precipitation anomalies is above 0.5 over the Southern Hemisphere, about 0.40–0.45 for the zone 30°–80°N, and only about 0.3 for 0°–30°N (Fig. 3). Since much of the area in northern middle to high latitudes (e.g., the United States and Europe) was covered by dense networks of stations, the areal precipitation anomalies of these regions are less sensitive to the choice of an influence radius if inverse distance weighting is used in the averaging. There were sparse networks of stations over the Southern Hemisphere, and the areal coverage there is more dependent on the radius. Putting all of these considerations together, we chose a single influence radius of 300 km for the global dataset because we were mainly interested in global and large-scale precipitation variations and wanted to keep the gridding of station data as simple as possible.

Figure 2 shows that during the maximum coverage period of 1951–70, about 85% of the land surface, or 40% of the global surface, was within 300 km of a station. This differs from station data of surface air temperatures, which are globally representative owing to the large influence radius (≈1200 km) in temperature anomaly fields (Hansen and Lebedeff 1987). The area within 300 km of a station was less than 40% of the global land area (approximately the current areal coverage) before this century. Therefore, we did not use data from before 1900.

3. Assessment and correction of inhomogeneity

Some analyses have suggested that the discontinuity errors could contribute a significant amount (up to 40%) to the observed precipitation variations at high-latitude stations (Alexandersson 1986; Groisman et al. 1991; Karl et al. 1993). However, their global significance has not been assessed. Statistical methods have been employed to detect and remove the inhomogeneities. Many of the techniques (e.g., Alexandersson 1986; Easterling and Peterson 1995; Easterling et al. 1996) are based on the assumption that a homogeneous reference series is available from surrounding stations. This is often not true in practice. The tests used by Eischeid et al. (1991) and Hulme (1992) do not provide a method to quantitatively correct the detected discontinuities.

In this study, we treat monthly precipitation anomalies at each station as 12 different time series and employ principal component (PC) analysis (Cooley and Lohnes 1971) to check whether any major common components exist in the 12 monthly time series of a station. Significant instrumental discontinuities should cause a stepwise component of variation (Karl et al. 1993) among the monthly time series independent of other climatic/nonclimatic variations. Principal component analysis can provide quantitative estimates of spurious precipitation caused by stepwise patterns and thus allow us to remove the discontinuity-induced errors from the time series. The identification procedure is greatly simplified by the fact that the discontinuity-associated PC should be of stepwise shape and be significant statistically (i.e., we are dealing only with those discontinuities that have significant impact on precipitation records).

Since the instrumental discontinuities generally occur on decadal time scales and our calculations showed that strong interannual variations of precipitation could obscure the low-frequency signals, we designed a seven-point Lanczos filter (Duchon 1979) with a cutoff period of 7 yr to remove multiyear variations in station time series prior to the PC analysis (note that total anomalies were used in the gridding and subsequent analyses). We then applied the PC analysis to the filtered time series of all stations having at least 20-yr records (stations with record lengths shorter than 20 but longer than 10 yr were used without the PC analysis). Of the 3543 stations tested, about 486 stations (≈14%) were found to have statistically significant PCs among their monthly time series [we used a two-tailed test based on North et al.'s (1982) sampling error estimates]. We further employed the Mann–Kendall rank sum test (Mann 1945; Kendall 1970) on the 486 stations' PCs to detect whether there was any jump (discontinuity) in these significant PCs. The rank sum test found that about 191 stations had at least one PC with likely discontinuities. We then visually examined the plots of the monthly time series and PCs for each of the 191 stations and concluded that only 92 stations had discontinuities of stepwise shape during this century. Since winter precipitation may have different discontinuities than those of summer precipitation due to phase changes in precipitation (solid vs liquid) (Karl et al. 1993), we also performed the PC analysis on winter and summer monthly precipitation separately. This analysis resulted in an additional 18 stations that had discontinuities of stepwise shape.

An example of the analysis is shown in Fig. 4 for a U.S. station (Bozeman, 45.7°N, 111.1°W). Plots of monthly time series of normalized precipitation anomalies seem to suggest an upward shift in the time series around 1970. However, the strong interannual variations within each monthly time series and the large intermonth variations tend to obscure the stepwise change. By applying the PC analysis to the (filtered) 12 monthly time series (specifically, each of the 12 89-yr-long monthly time series was treated as a separate column or variable in the data matrix; the resulting PCs are the common patterns among the 12 time series with different weights for different months), the stepwise shift hidden in the time series was successfully separated as the first leading PC from other components of variation (Fig. 4b). After removing the variations represented by the first PC (by subtracting the PC 1 component from the raw data), the adjusted the time series (Fig. 4c) were more homogeneous.

For area-averaged precipitation, there is another potential problem. While the PC analysis may suggest that instrumental discontinuities within the time series at individual stations are not significant, they could become a significant pattern when averaged over a region (e.g., within a country) because similar minor discontinuities might exist in many of the stations used in the averaging and their significance may increase as other rather random variations are smoothed out during the averaging. To address this problem, we examined the patterns of the first four PCs of all stations that were likely to have instrumental discontinuities, including stations in Europe, the former Soviet Union, China, Canada, and Alaska. Our results showed that stepwise patterns are generally found as the first or, occasionally, the second PC, and thus the examination of the first four PCs should be sufficient. This exercise resulted in an additional 46 stations that have moderate stepwise discontinuities and need adjustment.

Most of the stations (a total of 156) detected with

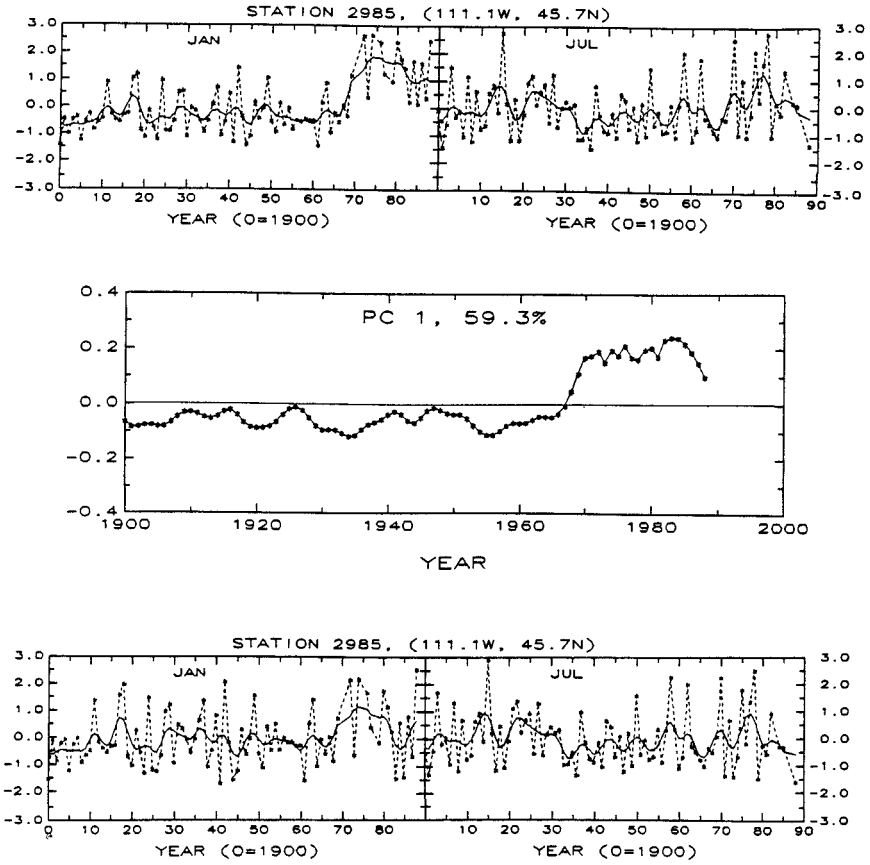

FIG. 4. An example of the instrumental discontinuity correction: (a) original time series of January and July precipitation anomalies (normalized by standard deviations) at U.S. station Bozeman (111.1°W, 45.7°N) (solid lines are filtered low-frequency variations), (b) the first leading principal component of the filtered variations of all monthly time series at the station, and (c) adjusted time series of January and July precipitation obtained by removing the variations represented by the discontinuity PC 1.

discontinuities are located in northern high latitudes, and the largest discontinuities were found in their winter precipitation, which is often in solid form and difficult to measure accurately and whose measurement is sensitive to instrumental designs due to the strong effect of winds on snowfall (Groisman et al. 1991; Groisman and Legates 1994). Therefore, it seems very likely that these discontinuities resulted from instrumental changes. We considered them as instrumental discontinuities in this study and removed them from their original time series using the discontinuity PCs. The adjusted station records were retained in subsequent analyses. Station records with lengths of 11–20 yr (~20%) were used without the inhomogeneity analysis.

Our analysis showed that the instrumental discontinuity is a more serious problem for former Soviet Union stations than for stations of other countries, presumably due to the large portion of solid precipitation at high latitudes. The analysis also indicated that major discontinuities for most Soviet Union stations occurred around 1950 when the Tretiyakov gauge, which measures solid precipitation more accurately than the old Nipher shielded gauge, was introduced (Groisman et al. 1991). The discontinuity adjustment reduces (by ~40% in annual precipitation) the rate of increase of area-averaged precipitation over former Soviet Union territory from the 1940s to the early 1950s. The impact of the adjustments are insignificant in area-averaged precipitation over other regions, although the adjustments were large for a small number (≈25) of Canadian and U.S. stations.

The above results are consistent with the findings of previous studies (Eischeid et al. 1991; Hulme 1992) and suggest that for the majority of the stations there are no major stepwise discontinuities. This is probably also true for large-area-averaged precipitation because (minor) instrumental discontinuities are not always in phase over a large area (e.g., over several countries). However, the technique used here has its limitations. First, for stations with short records, the PC analysis is not accurate, although the probability that those stations had instrumental changes is generally smaller than that for stations having a longer length of records. Second, while it may be easy to identify a major discontinuity from the PCs, small instrumental discontinuities could still

exist in station records after the correction, although they are unlikely to be important.

4. Spatial averaging and sampling errors

Because of the irregularity in station distribution, gridding is needed to reduce regional bias in area-averaged precipitation. There are a number of widely used methods in hydrologic studies for estimating short-time (e.g., hourly) areal precipitation from dense station networks [e.g., the Thiessen polygon method, the Kriging method, and Gandin's optimal method; see, e.g., Creutin and Obled (1982); Lebel et al. (1987)]. Here we employ a simple distance-weighted averaging to combine the station data since monthly precipitation is much less variable than short-time rainfall and our object is to estimate large-scale ($\sim 10^3$ km) variations. Since much of the spatial variation of precipitation is associated with local orography (Cotton and Anthes 1989) and is thus steady and depicted in climatological maps of monthly precipitation (e.g., Shea 1986), we first subtracted monthly mean climatologies from total precipitation fields and interpolated the residuals onto a 2.5° × 2.5° grid using the following distance-weighted scheme:

$$\Delta P_n = P_n - P_{no}, \tag{1}$$

$$\Delta P_{ij} = \frac{\sum_n w(r_n)\Delta P_n}{\sum_n w(r_n)}, \tag{2}$$

and

$$w(r_n) = 1 - r_n/d \quad \text{if } r_n < r_0$$

and (3)

$$w(r_n) = 0 \qquad \text{if } r_n \geq r_0,$$

where P_n is the monthly total precipitation at station n, P_{no} is the climatological (1950–79) value of P_n at the station, ΔP_{ij} is the gridded precipitation anomaly at grid point (i, j), r_n is the distance between station n and the center of grid box (i, j), r_0 is the influence radius (=300 km), and d is a constant (=880 km). The summation in (2) includes all stations within the influence radius. The weighting function $w(r_n)$ and constant d were chosen to fit the mean shape of the correlation curves in Fig. 3. We tested other forms of $w(r_n)$ [e.g., $\exp(-r_n/c)$, $1 - r_n^2/c$, $1/r_n$, and $r_n^{-1/2}$, where c = constant] and found that the gridded precipitation anomalies are insensitive to the choice of the weighting function, with a grid resolution of 2.5° and an influence radius of 300 km.

Spatial sampling errors are introduced (especially across mountains) by using ΔP_{ij} as estimated from (2) to represent areal precipitation anomalies of the grid box. First, consider two nearby stations inside a grid box that have a correlation coefficient ρ between their time series of precipitation. Since a squared correlation coefficient represents the percentage of the total variance of one variable explainable by the other, the spatial sampling error (e_s) induced by using a station record (station 1) to represent the precipitation at the other station (station 2) may be estimated as $(1 - \rho^2)^{1/2}\sigma_2$, where σ_2 is the standard deviation of precipitation at station 2.

Next, let us consider the sampling error induced by using a station record to represent the precipitation anomaly (ΔP_A) of an area A around the station. The percentage (α_A) of the precipitation variance of the area that is not accounted for by the station record may be estimated using

$$\alpha_A^2 \approx \int_A [1 - \rho(r)^2]\, dA/A, \tag{4}$$

where ρ(r) is the spatial correlation function of precipitation anomalies at two locations separated by a distance r. Using the mean shape of ρ(r) for global land precipitation, shown in Fig. 3, we estimate that α_A is about 20%, 27%, and 38% for a circular cell with a radius of 30, 50, and 100 km, respectively. The absolute sampling error of ΔP_A is $\alpha_A\sigma_A$, where σ_A is the standard deviation of ΔP_A.

Now, consider a grid box consisting of N subgrid boxes, each having an area of A and containing a single station. Since the precipitation anomaly for the grid box (ΔP_{ij}) is a linearly weighted average of all ΔP_A's [cf. Eq. (2)] and the sampling errors in each ΔP_A are independent, the sampling error in ΔP_{ij} is about $\alpha_A\sigma_{ij}N^{-1/2}$, according to the Central Limit Theorem (Mendenhall et al. 1990) (σ_{ij} is an averaged value of all σ_A and close to the standard deviation of ΔP_A)—that is, the percentage of the sampling error of ΔP_{ij} (α_{ij}) is about $N^{-1/2}$ times that of ΔP_A.

The average number of stations (N) per 2.5° × 2.5° grid box during most of the time from 1900 to 1988 is about 10 in the United States and southern Canada; 6 in Europe, eastern Australia, and the Sahel; 7 in southern Africa; and less than 5 for other regions. At such levels of station density, α_A is ~25% for $N = 10$, 29% for $N = 7$, 30% for $N = 6$, 31% for $N = 5$, and 45% for $N = 1$. The respective α_{ij} (i.e., the percentage of the sampling error of gridded anomalies) are ~8%, 11%, 12%, 14%, and 45%. Thus, the sampling error in gridded precipitation anomalies at 2.5° × 2.5° resolution is around 10% for the well-covered regions including the United States, southern Canada, Europe, eastern Australia, the Sahel, and southern Africa, but as high as 45% in other poorly covered areas. The above estimates of the sampling errors are consistent with those obtained from an intercomparison of gauge observations and satellite estimates of monthly precipitation (Xie and Arkin 1995).

Since α_A is a function of station density and precipitation variance does not vary dramatically over most of the land areas except the edges of arid areas, the sampling errors of regional precipitation anomalies will

decrease approximately with $N^{-1/2}$ as the area of the region increases. For example, even if each 2.5° × 2.5° grid box contains only 1 station (i.e., α_A is ~45%), the area-averaged anomalies over 10 adjacent grid boxes will generally have a sampling error of about 14%. As a compromise between computational and resolution requirements, we used a 2.5° × 2.5° grid in this study. At this resolution, long-term or large-scale signals are not likely to vary significantly inside each grid box, while the number of stations involved in deriving ΔP_{ij} [cf. Eq. (2)] is large enough to reduce the spatial sampling error significantly, at least for the well covered areas. However, for those areas with only 1 or 2 stations inside or around each grid box, such as northern Russia, northern and central South America, northern North America, northern Africa, and the Middle East, the spatial sampling error for each grid box could be as high as 45%. In these areas, only those regional signals covering 10 or more grid boxes (more at high latitudes, where the grid boxes are smaller) should be considered meaningful. In addition, the 300-km gridding radius limits the dataset to examining variations with spatial scales greater than several hundred kilometers.

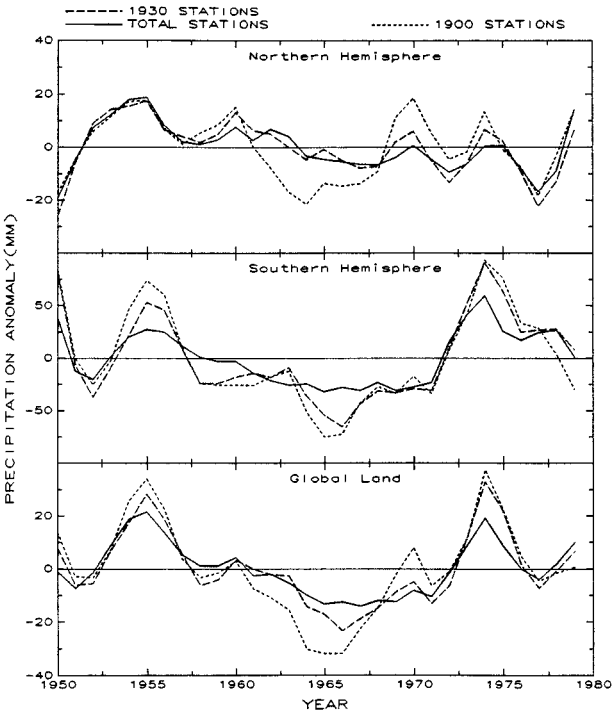

FIG. 5. Precipitation anomalies (3-yr mean) of the period 1950–79 over global and hemispheric land areas estimated using precipitation records from all available stations (solid line) and only the stations that existed in 1900 (dashed line) and 1930 (broken line).

5. Validation of the gridded dataset

The major sources of error in the gridded precipitation dataset include instrumental errors, limited station coverage, and errors induced during the interpolation/gridding. The instrumental errors include a systematic bias (undercatch), which should have relatively small effects on the variation patterns, and inhomogeneity, which, as shown in section 3, is not a major component of variation at most of the stations. Our PC-based adjustment has improved the homogeneity of the data in the worst cases.

One estimate of the magnitude of the station-coverage-induced error is illustrated in Fig. 5, in which we compare the globally and hemispherically averaged precipitation of 1950–79 with versions that are sampled using only the stations that existed in 1900 and 1930, when station coverage was much lower (cf. Fig. 2). Figure 5 shows that poorer station coverage tends to produce larger amplitudes of area-averaged precipitation anomalies. Most of the major features of global and hemispheric precipitation change can be seen in the sampled datasets. The main exception is that the 1900 station coverage fails to capture the decreasing trend over the Northern Hemisphere during the period.

Another test of the gridded dataset is whether it is consistent with other independent information relevant to precipitation. We compared our precipitation anomalies of the 1970s and 1980s with the flood and drought reports in *Climate Monitor* and the seasonal climate summary reports in *Monthly Weather Review* and *Journal of Climate*. General agreement was found between the gridded precipitation maps and the regular climate reports. Flood and drought occurrences associated with ENSO events (Rasmusson and Carpenter 1982; Ropelewski and Halpert 1987, 1989) are especially prominent in an EOF analysis of the gridded precipitation data (see section 7 for details). The recent sub-Saharan drought condition is also shown by the gridded data when compared with previous studies [e.g., Lamb and Peppler 1992; Nicholson 1993].

Precipitation is physically related to clouds and positively correlated with the amount of middle-and high-level cloud cover (Arkin 1979; Richards and Arkin 1981; Dai et al. 1997). Figure 6 shows the relationship between annual precipitation and total cloud cover, which was taken from Henderson-Sellers (1992) and Karl and Steurer (1990) and has its own errors (which are uncorrelated with the errors in precipitation) over western (west of 40°E) Europe, the contiguous United States, midlatitude Canada, India, and Australia. The correlation between the two records is far from perfect, as would be expected since total cloud cover includes nonprecipitating as well as precipitating clouds, but the records appear to covary in general, indicating that the long-term (as well as the multiyear) variations of precipitation (at least when averaged over continental areas) are likely to be real.

The above analyses show that, despite the limited spatial coverage of the stations and the various instrumental errors in rain gauge records, precipitation

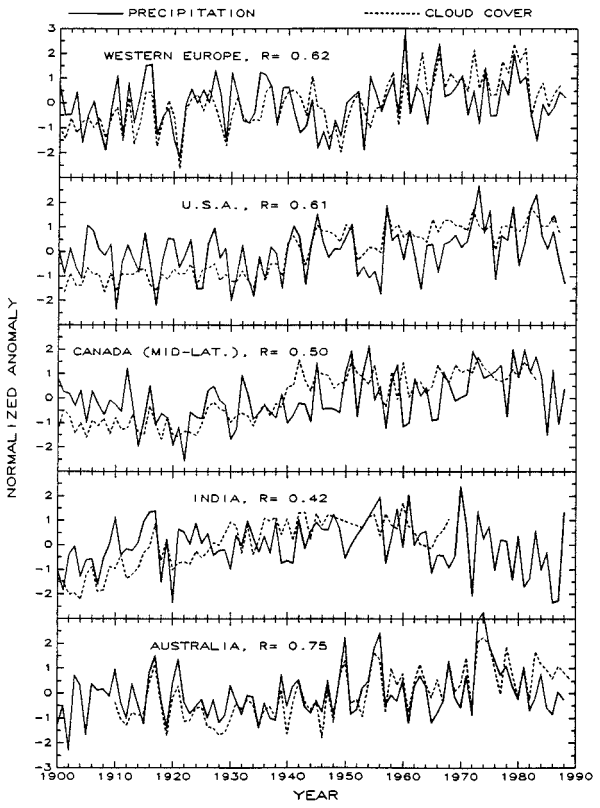

FIG. 6. Relationship between continental precipitation (solid line) and cloud cover (dashed line). The cloud cover data are from Henderson-Sellers (1992) and Karl and Steurer (1990). Here R is the correlation coefficient between the two curves.

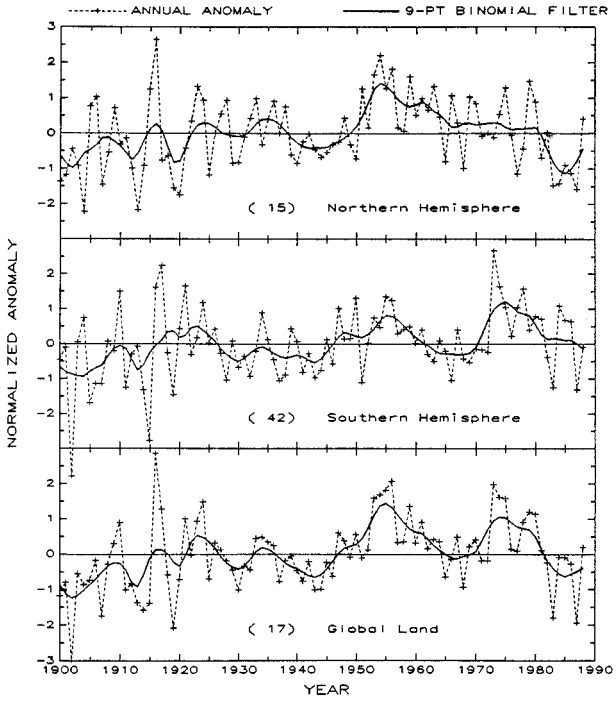

FIG. 7. Normalized annual precipitation anomalies (zero line is the 1900–88 mean) of hemispheric and global land areas. The solid lines are smoothed values obtained using an improved nine-point binomial filter. The anomalies are derived from the gridded dataset, which has no data over open oceans (cf. Fig. 1) using area-weighted averaging. The numbers in parentheses are the standard deviations of the curves (in millimeters) used in the normalization.

changes of large regions derived from the gridded dataset appear to be meaningful.

6. Global and zonal precipitation changes

The major patterns in global and hemispheric (Fig. 7) and zonal (Fig. 8) precipitation are similar to those found in previous analyses (Bradley et al. 1987; Diaz et al. 1989; Vinnikov et al. 1990; Nicholls and Lavery 1992; Groisman and Easterling 1994]. However, our results do not show an increasing trend as remarkable as that of Diaz et al. (1989) over Southern Hemisphere land areas during the last 3–4 decades. We believe that our results are more reliable because Diaz et al. (1989) have only a few stations over central Africa and northern and central South America. In general, global precipitation was relatively stable, or increased slightly from 1900 to the early 1940s. It then increased sharply from the mid-1940s to the mid-1950s and has stayed relatively high since then over most of the land areas except the Tropics, where land precipitation decreased to below the 1900–88 mean in the 1970s and 1980s. There is also a general decreasing trend in precipitation since the late 1970s over all latitudes south of ~60°N. The 40°–60°N increasing trend is most pronounced in March–May precipitation, whereas the 0°–20°N decreasing trend is most evident in June–August precipitation and least seen in December–February precipitation.

The above-normal anomalies of the period of 1950–79 in global precipitation (Fig. 7) do not appear to be an artifact of the increase in the number of stations during this period (cf. Fig. 2). As shown in Fig. 5, the higher station coverage of the period of 1950–79 does not induce any systematic bias relative to lower station coverage, although the increase of station coverage results in slightly smaller magnitudes of (both positive and negative) anomalies. Mathematically, precipitation anomalies averaged over the newly expanded coverage (~20% of the global land areas, cf. Fig. 2) during the period of 1950–79 should have a zero mean when they are averaged over the period of 1950–79 since the gridded anomalies are relative to the 1950–79 mean [cf. Eqs. (1)–(3)]. It follows that the systematic increase of precipitation of the period of 1950–79 over the period of 1900–49 can only result from the areas covered during both of the periods. Diaz et al. (1989), who selected 1921–60 as the reference period, and Eischeid et al. (1991), who used 1951–70 as the reference period, find a similar upward shift of precipitation for the period of 1950–79.

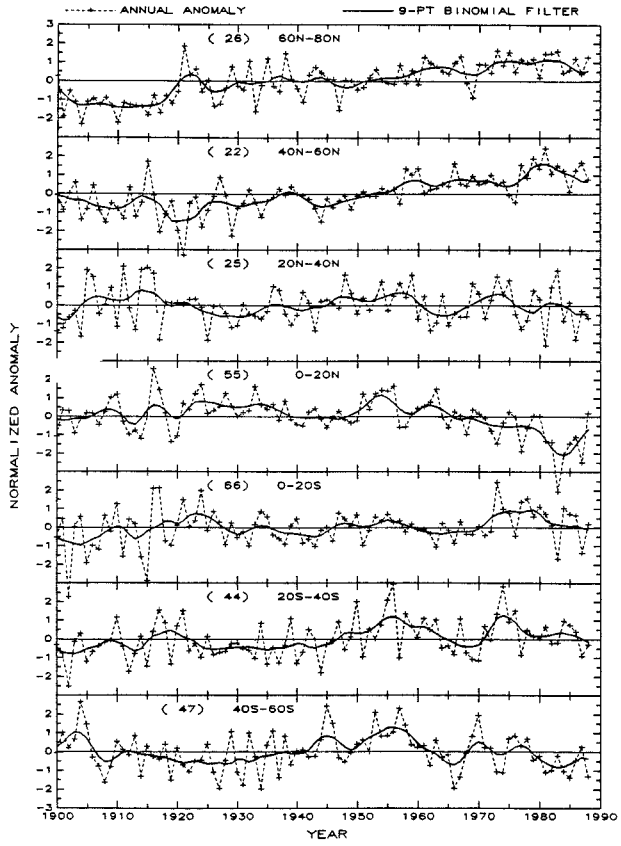

FIG. 8. Same as in Fig. 7 except averaged over 20° latitude zones.

7. Temporal and spatial structures of precipitation variation

In this section, we examine the temporal and spatial structures of global precipitation fields using EOF analyses (Kutzbach 1967; Wallace and Gutzler 1981; Wallace et al. 1993). The gridded anomalies are first normalized by their standard deviations prior to the EOF analyses. Gridded anomalies of less than 11 yr in length are not used in the analyses. We first performed an EOF analysis on the global dataset to obtain globally significant modes. While the global analysis can capture the most important modes in global precipitation fields, it is likely to miss many regional modes (cf. section 7c), and, more seriously, physically unrelated regional patterns may be blended together to produce artificial global modes if the signals are weak and sampling errors are large. To partly solve the problem, we also performed EOF analyses of precipitation on regional domains to identify regional leading modes. The significance of the leading modes was established mainly based on the physical signals contained in their temporal and spatial patterns, although statistical tests were also performed (Dai 1996). The stability of the modes in repeated EOF analyses of subsets of the dataset was also examined and used as one of the indications of significance. For example, EOF 1 (ENSO signal) of the whole global dataset is seen in separate EOF analyses for the periods of 1900–49 and 1939–88 and low latitudes (30°S–30°N). The ENSO signal is also seen in EOFs of seasonal precipitation. The second EOF (trend signal) of the global dataset is seen in EOFs for the period of 1939–88 and northern middle to high latitudes. More convincingly, the trend signal is seen in the regionally averaged precipitation anomalies (i.e., raw data) over North America, northern Eurasia, Australia, and Argentina, where the second EOF is most significant (Dai 1996). Globally, only the first two EOFs are separated reasonably well with respect to sampling errors (North et al. 1982) and are relatively stable, but several significant regional EOFs were identified as well.

The EOFs are the mean spatial patterns of the period of 1900–88. The temporal coefficients (PCs) are the mean signal averaged over the EOF maps. For a particular year, the corresponding (normalized) anomalies are the product of the temporal (PC) and spatial (EOF) coefficients. Since not all the grid boxes have data back to 1900 (cf. Fig. 1), the number of actual years used in deriving the spatial (EOF) coefficients is considerably shorter than 89 for many high-latitude areas, for central Asia, and for central Africa. However, for most of the active regions of the two leading EOFs discussed below, the sampling length is in the range of 80–89 yr.

a. EOF 1—ENSO signal in global precipitation fields

The time and space components of the first leading EOF (EOF 1) of annual precipitation anomalies are shown in Fig. 9. The time component of EOF 1, which accounts for ~6.3% of the total variance, replicates the ENSO cycles in the equatorial Pacific SST in the domain of 6°S–6°N, 90°–170°W; 6°S–2°N, 170°–180°W; and 6°–10°S, 110°–150°W (Wright 1984), indicating that EOF 1 is related to ENSO. The major low-latitude patterns of EOF 1 are similar to those found by Lau and Sheu (1988) and Ropelewski and Halpert (1987, 1989). However, Fig. 9 also suggests that precipitation in some midlatitude regions (namely, western Canada, central western Europe, and central Eurasia) is also affected by ENSO. Figure 9 shows that while most of the variations are of multiyear timescales, there is also some decadal variability associated with the ENSO-related EOF patterns. Also, although ENSO-related regional precipitation can be large, the ENSO signal in globally averaged land precipitation is only about 10–30 mm, or 1%–4% (a decrease during El Niños), because many of the ENSO-related regional precipitation anomalies result from shifts of precipitation centers from one region to another, which generate both positive and negative anomalies (Fig. 9).

EOF analyses of seasonal precipitation revealed that the ENSO signal is the first leading EOF in all seasons. The ENSO EOFs of seasonal precipitation (Dai 1996) show that the ENSO-induced precipitation anomalies in the Australia–Indonesia region generally reach a max-

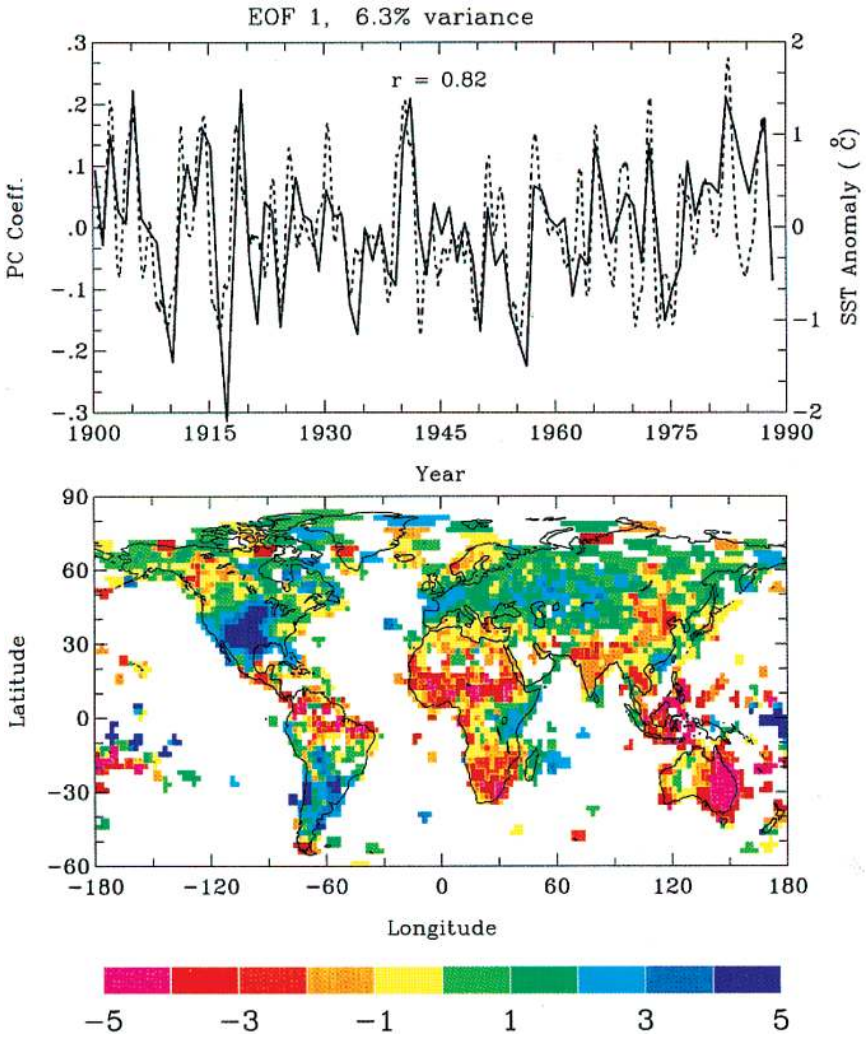

FIG. 9. Temporal coefficients and spatial patterns of the first leading EOF of annual precipitation anomalies (normalized by their standard deviations prior to decomposition). Also shown (dashed line) is the bimonthly SST anomalies over the equatorial Pacific (Wright 1984). Areas without data are in white. The annual PC coefficients (top panel, solid line) were plotted at the SON of each year (e.g., 1982 PC coefficient is plotted at x axis = 1982.75 instead of 1982.50) since the largest ENSO-induced precipitation anomalies are generally in SON (Dai 1996).

imum in September–November (SON) of the ENSO year and recover to normal in the following March–May (MAM), while the anomalies over the United States are seen mostly during December–February (DJF) and MAM following the ENSO year (e.g., 1983). These results are consistent with those from composite analyses (Ropelewski and Halpert 1987, 1989).

We find that the strength of the ENSO signal in precipitation is season dependent, and this seasonality varies from region to region. For example, in North America, the ENSO signal in precipitation is strongest in winter (DJF) and weakest in summer [June–August (JJA)], whereas in the Australia–Indonesia region, ENSO affects precipitation most in SON and least in MAM. Globally, the ENSO signal is strongest in SON (7.5% variance) and weakest in JJA (5.1% variance). This is understandable because the equatorial Pacific SST is still warming up during JJA in a typical El Niño year and reaches a maximum in SON, and atmospheric circulation anomalies associated with the ENSO SST anomalies are the major (initial) cause for the observed dramatic precipitation changes in the Tropics and midlatitudes during ENSO years (Rasmusson and Carpenter 1982; Trenberth and Guillemot 1996).

We also find that ENSO is not a significant mode of precipitation variation for northern mid- to high latitudes (40°–75°N), while it is the first leading mode and accounts for ~9% of the total variance of annual precipitation in low latitudes (30°S–30°N, mostly land).

From the perspective of monitoring non-ENSO signals such as anthropogenic greenhouse effects in global precipitation fields, the above seasonality of the ENSO

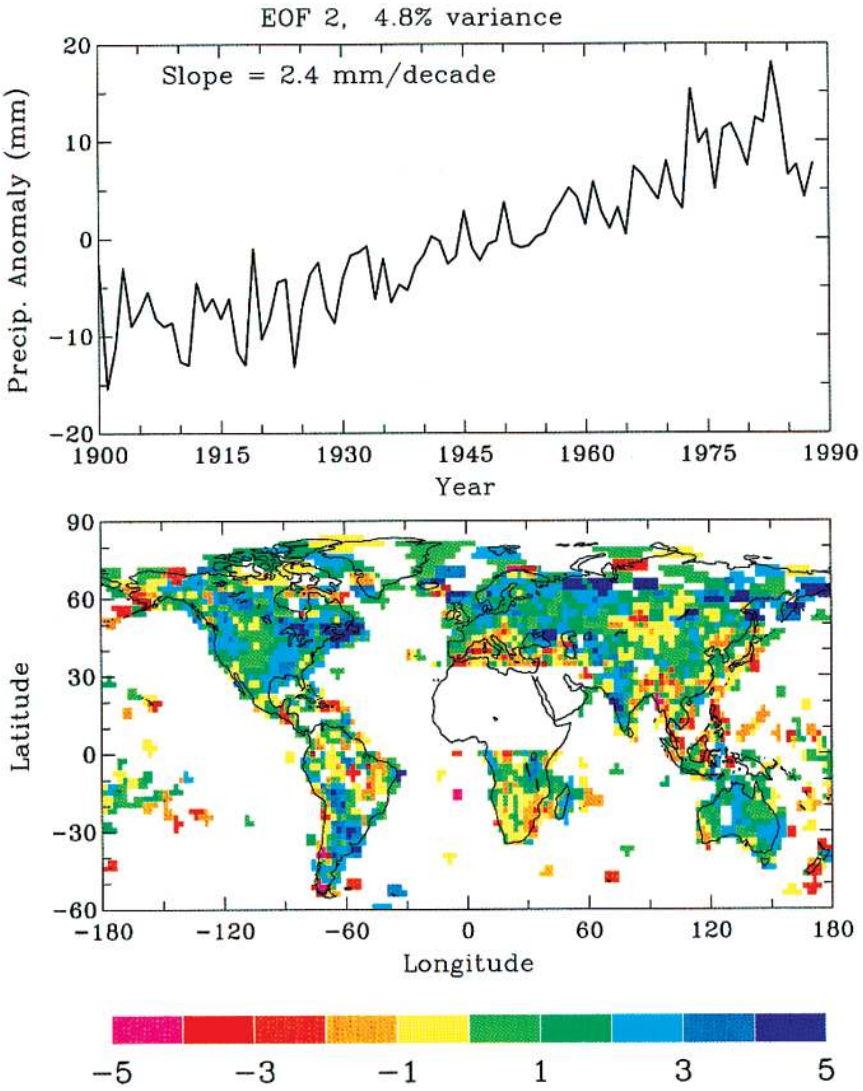

FIG. 10. Temporal coefficients and spatial patterns of the second leading EOF of annual precipitation anomalies over the globe, excluding northern Africa. Note that the coefficients are converted into globally aggregated precipitation anomalies associated with the EOF. Areas without data are in white.

signal has practical implications. For example, it is better to monitor MAM rather than SON precipitation in Australia and JJA instead of DJF precipitation in North America for secular precipitation trends (the seasonality of the trends is relatively small). Decadal- to century-scale variability also stands out more clearly in the warm season time series of surface air temperature (Wallace et al. 1996).

b. EOF 2—A secular increasing trend

The second EOF of the global precipitation field shows a linear trend, with increases over northern mid-latitudes and large decreases in the sub-Sahara from 1900 to 1988. Since it is well established that sub-Saharan rainfall has been decreasing only since the 1950s (Lamb and Peppler 1992; Nicholson 1993) and a separate EOF analysis of northern Africa failed to show any linear trends [while ~16% of the total variance of annual precipitation in the region was accounted for by a decadal mode (EOF 1) that depicts decadal variations in sub-Saharan rainfall (Lamb and Peppler 1992)], this linear trend is an incorrect depiction of long-term precipitation changes in the sub-Sahara. Thus, we excluded northern Africa and repeated the EOF analysis in which we obtained a second EOF (Fig. 10) whose patterns are similar to that of the global (including northern Africa) analysis.

Figure 10 shows that, temporally, EOF 2 is a linear trend and, averaged over the globe, it is an increasing

trend (≈2.4 mm decade^{-1}); spatially, it occurs fairly uniformly over most of the middle- and high-latitude land areas. Over some parts of the low latitudes (the Philippines, Malaysia, and the Mediterranean), EOF 2 represents a long-term decrease of precipitation.

Figure 10 suggests an increasing trend over North America, mid- to high-latitude Eurasia, Australia, and Argentina. Plots of annual precipitation averaged over the above four regions confirmed the trend (Dai 1996). Plots of seasonal precipitation further showed that increasing linear trends are evident mostly in SON and JJA for North America, and in all four seasons for Eurasia and Argentina. They are weak in all the seasons for Australia. The trend signal is much weaker and less identifiable among the EOFs of seasonal precipitation.

An EOF analysis for northern mid- to high latitudes (40°–75°N) revealed that the combination of the first two leading EOFs matches the temporal and spatial patterns of the trend EOF shown in Fig. 10 well. An EOF analysis for low latitudes (30°S–30°N) showed a moderate upward trend, with spatial patterns similar to those in Fig. 10.

One of the possible causes for the secular trend depicted by the second EOF (Fig. 10) is global warming. Analyses of station records have shown that during the last 100 yr globally averaged surface air temperature has increased by ~0.45 ± 0.15°C (Hansen and Lebedeff 1987, 1988; Jones and Briffa 1992; Vinnikov et al. 1990; IPCC 1990, 1992, 1996). The warming is also supported by evidence of increasing water vapor in the troposphere since the mid-1970s in the Tropics (Elliott et al. 1991; Gaffen et al. 1991), in North America (Ross and Elliott 1996), and in other regions (Gaffen et al. 1992). Atmospheric thermodynamics suggests that surface warming should increase surface evaporation and evapotranspiration, all other things being equal. On decadal timescales and when averaged globally, this increase should be approximately balanced by similar increases in precipitation [note that atmospheric total precipitable water content is only about 30–70 mm (Greenwald et al. 1993), or ~5% of globally averaged annual precipitation]. Therefore, the increasing trend represented by the second EOF is thermodynamically consistent with the observed global warming.

Both equilibrium doubled CO_2 and transient greenhouse gas simulations with global climate models generally produce increased precipitation in middle to high latitudes and decreased precipitation over low-latitude land areas in warmer climates, although large differences exist among different GCMs (IPCC 1996). Although regional differences have been reported in the responses of the climate system to a doubling of atmospheric CO_2 in equilibrium atmospheric GCM and fully coupled transient ocean–atmosphere GCM experiments (Washington and Meehl 1989; Manabe et al. 1992; IPCC 1992), the general patterns of precipitation changes due to a doubling of CO_2 are similar in the two kinds of experiments (IPCC 1996). The observed trend is a transient response and qualitatively consistent with the GCM results in sign and general geographic patterns (note that EOF 2 suggests a weak decrease of precipitation over some parts of the low latitudes besides the decreasing trend over northern Africa during recent decades). The observed rate of increase (~2.4 mm decade^{-1}) is also comparable to that (~3.0 mm decade^{-1}) from a 1% yr^{-1} CO_2 increase simulation in a coupled ocean–atmospheric GCM study (Russell et al. 1995).

c. North Atlantic oscillation (NAO) signal in precipitation fields

The above EOF analyses aim to delineate modes of global significance. Here, we present results of an EOF analysis of precipitation over the North Atlantic surrounding region (20°–80°N, 90°W–40°E). Figure 11 shows the temporal and spatial patterns of the two leading EOFs of DJF precipitation over the North Atlantic region. The first EOF, which has considerable power at timescales of about 11 yr and accounts for 12.3% of the total variance, exhibits an alternating pattern in latitude over Europe (high in central Europe and low in northern Europe, the Mediterranean, and northern Africa). This pattern is seen in all seasonal and annual precipitation, although it is most pronounced in winter months. Deser and Blackmon (1993) have reported an EOF pattern in North Atlantic sea level pressure and surface zonal wind that has considerable power at 9–12-yr timescales and depicts anomalous westerlies at 45°–60°N latitudes across the North Atlantic. EOF 1 of Fig. 11 seems to be linked to this EOF mode in surface circulation fields over the North Atlantic.

The second EOF has highest power around the 7-yr timescale and accounts for about 10% of the total variance. Its temporal coefficient correlates significantly with an NAO winter index, defined as the difference in normalized pressures between Lisbon, Portugal, and Stykkisholmur, Iceland (Hurrell 1995). The spatial patterns of EOF 2 match the composite NAO precipitation anomaly patterns inferred by Hurrell (1995) based on atmospheric moisture convergence. Thus, the second EOF is likely caused by the anomalous moisture transport/convergence associated with the NAO circulation. EOF 2 (Fig. 11) suggests that during high-NAO-index winters, precipitation tends to be 0.5–1 σ above normal in northern (>~50°N) Europe and the eastern United States, and about 0.5 σ above normal in northern Africa and the Mediterranean; while southern Europe likely receives 0.5–1 σ below-normal precipitation. Drier conditions also occur during high-NAO-index winters from eastern Canada to western Greenland.

8. Extreme precipitation

Droughts and floods are two extremes of precipitation variability. These extreme precipitation events are usually associated with large (in terms of both spatial scale

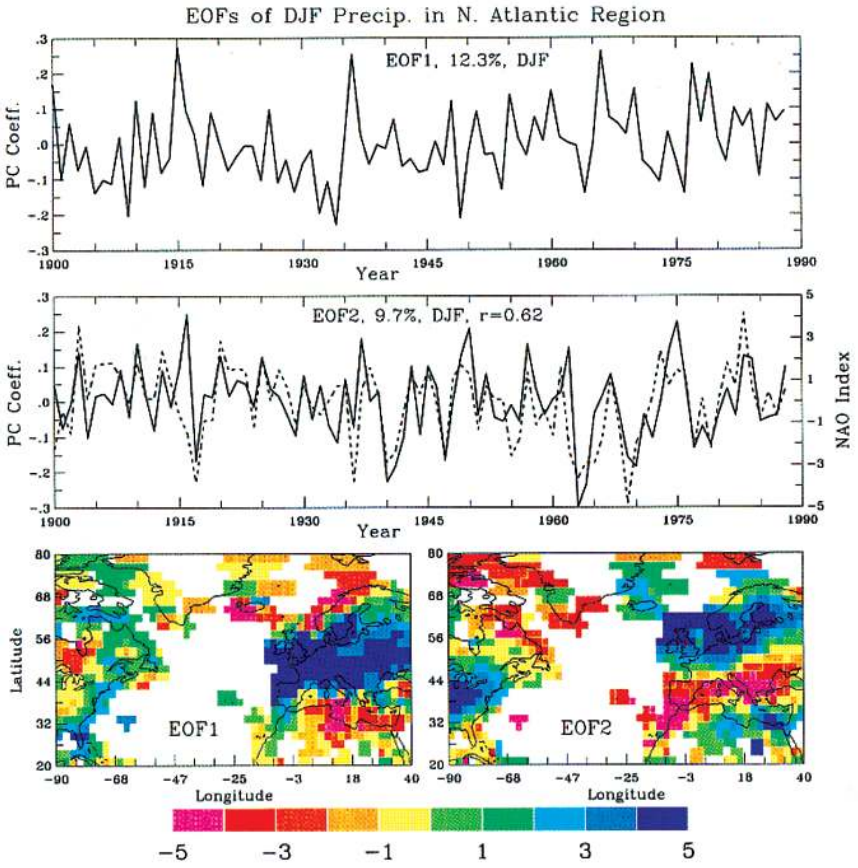

FIG. 11. First two leading EOFs of DJF precipitation in North Atlantic surrounding regions. Upper and middle panels: EOF temporal coefficients. Lower panels: EOF spatial patterns. A winter NAO index (Hurrell 1995) was plotted (dashed line) with EOF 2 in the middle panel.

and magnitude) anomalies in the atmospheric circulation, and the resulting anomalous surface conditions may amplify and prolong the perturbations (Namias 1983; Trenberth and Guillemot 1996). Most previous studies on droughts or floods have been case analyses and have often focused on a particular region. In this section, we describe some of the statistical characteristics of extreme precipitation events over the global land areas derived from the gridded dataset of the period of 1900–88. Our focus is on the mean behavior and large-scale patterns of the extreme events. Our analysis also provides a global, long-term context with which to view recent well-publicized anomalies, such as the 1988 drought and 1993 floods in the Midwest. Two kinds of extreme precipitation events are examined here: 1) dry or wet events, which are defined as the months having precipitation more than one standard deviation (σ) below or above normal (the 1950–79 mean), and 2) severe dry or wet events, which are defined as the months having precipitation more than 1.5 σ below normal or more than 2.5 σ above normal. The σ thresholds were chosen mainly based on the probabilities of occurrence of the events and the skewness of the histograms of monthly precipitation time series.

To characterize the extreme precipitation events, we calculated the mean duration of wet and dry events. We found that the mean duration of the 1 σ wet and dry events has little spatial variability ($<$1 month) over the globe. About 80%–85% of the wet or dry episodes last only 1 month, and about 12%–16% of these events persist for 2 months. Fewer than 5% of the extreme precipitation events last longer than 2 months. The mean of the duration is about 1–1.5 months, with a standard deviation of $\sim$0.5 months. The duration statistics vary little from the period 1900–44 to the period 1945–88.

We then examined the mean separation time between two adjacent extreme events (please note that ''2 consecutive months'' is defined here as having a separation interval of 1 month). Figure. 12 shows the distributions of the mean time interval between two adjacent wet, dry, severe wet, and severe dry months. It can be seen that in northern midlatitudes the mean wet-to-wet (w-w) interval is around 5–7 months. It increases to around 8 months in the arid areas in central Asia. In desert areas

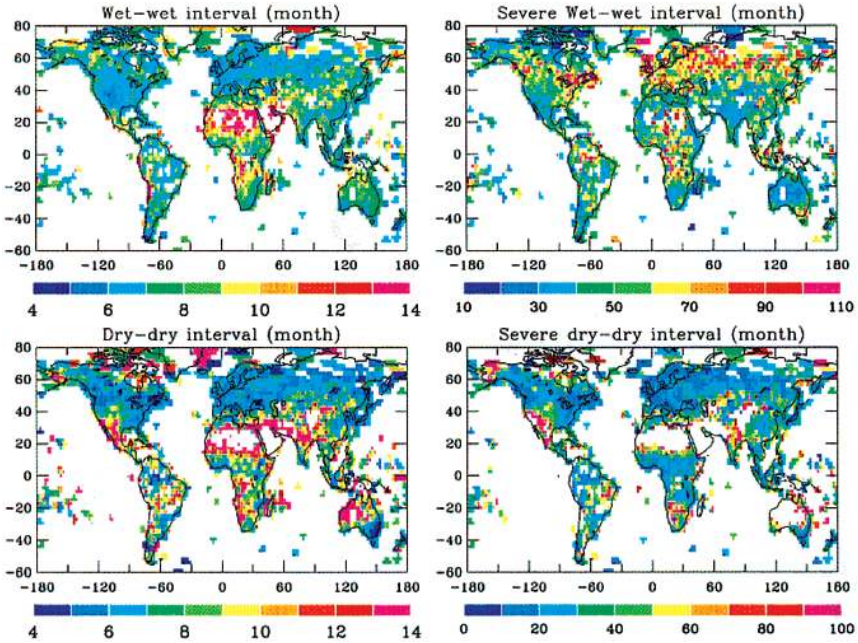

FIG. 12. Distribution of the mean time interval between 2 adjacent wet (>1 σ), dry (<−1 σ), severe wet (>2.5 σ), and severe dry (<−1.5 σ) months.

of northern Africa and the Middle East, the mean w-w interval ranges from 11 to over 14 months. Large mean w-w intervals (10–13 months) are also seen in central Africa and northern Chile. In most of South America and Australia, the mean w-w interval is around 7 months. The mean w-w interval over the islands and coastal areas is similar to that over inland regions.

The mean dry-to-dry (d-d) interval is fairly uniform (around 6 months) in mid- and high latitudes. In the subtropics, the mean d-d intervals are considerably higher (>12 months) than those in midlatitudes.

The mean w-w and d-d intervals are indicative of the occurrence probability of the wet and dry months. For example, on average, dry months occur about once every 6 months in midlatitudes, suggesting an occurrence probability of ~16.7% for the dry events. For the wet events, the occurrence probability is about ~14.3% in midlatitudes. These probabilities are close to the $1 - \sigma$ probability of a normal distribution (~15.87%), indicating that the histograms of monthly precipitation in midlatitudes are only slightly skewed. The histograms of monthly precipitation in subtropical regions (e.g., the Sahara and central Australia) are skewed and more peaked than normal so that there are lower probabilities on both tails of the histograms than those that a normal distribution would predict.

The mean spatial patterns of the interval between severe (<−1.5 σ) dry events are similar to those of the l-σ dry events, with timescales of ~10–30 months in midlatitudes and ~40–70 months in northern India and some arid areas. The mean spatial patterns of the interval between 2.5-σ wet events (Fig. 12) are, however, very different from those of the 1-σ wet events. Figure 12 shows that the severe wet months occur once about every 50–110 months in the northern midlatitudes, northern South America, and central Africa, and once about every 30–50 months in India, the Mediterranean region, and Australia.

The 1σ wet-to-dry and dry-to-wet intervals exhibit small spatial variability (<4 months). The mean separation interval is about 3.7 months averaged globally, which is about half that of the mean w-w or d-d interval. It is slightly higher in subtropical arid areas.

Globally, from the period 1900–44 to the period 1945–88 the mean (1 σ-) dry-to-dry interval increased by ~2.4 months, or 28%, while the mean (1 σ-) wet-to-wet interval decreased only slightly (~3%). These changes are consistent with the upward trend in global precipitation during this century (cf. Fig. 7).

Figure 13 shows the percentages of areas and severity (expressed in areal average of normalized anomalies) of wet (>1 σ) and dry (<−1 σ) events (relative to the 1950–79 mean) over different regions from 1900 to 1988. The wet and dry percentage areas for the globe (Fig. 13, top panels) are strongly influenced by the total sampling areas (cf. Fig. 2). For the other three regions [the United States, western (20°W–30°E) Europe, and Australia], station coverage has been relatively stable during the period 1900–88 (cf. Fig. 1) and should have small effects on the percentages of areas. The area and severity of wet and dry events are positively correlated (except for the wet case over western Europe). For the United States, the wet areas have more than doubled (from ~12% to <24%) since the 1970s, while the dry

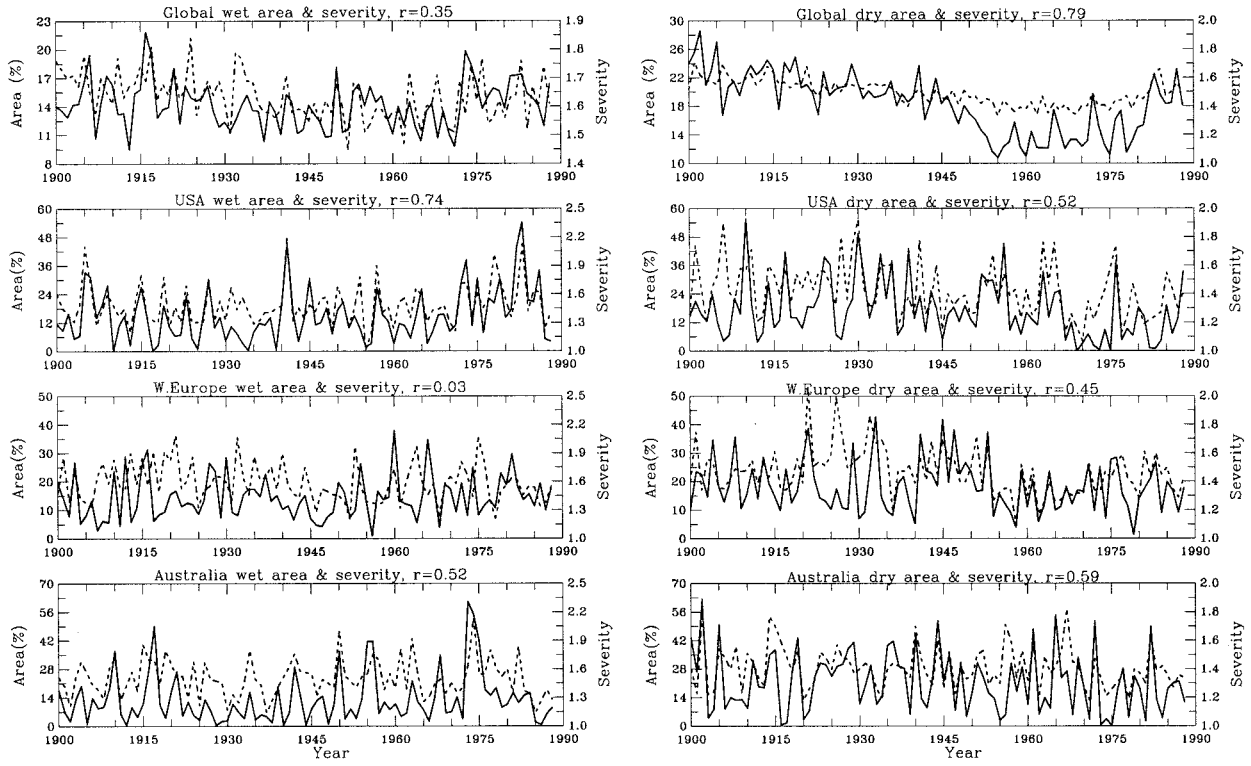

FIG. 13. Percentages of areas (solid line) where annual precipitation is at least one standard deviation above (wet, left column) or below (dry, right column) the 1950–79 mean. Also shown are the area-averaged magnitude (severity, dashed line, in units of std dev) of the wet and dry anomalies. The results, which are calculated at 2.5° × 2.5° resolution, for the globe and regions with good station coverage during this century are plotted separately.

areas have decreased by a similar amount since the 1940s. The wet severity has increased by ~0.3 σ, while the dry severity has dropped a comparable amount since the 1940s over the United States. Similar trends are also seen over Australia. In western Europe, however, only the dry areas and severity decreased slightly over the last 4 decades.

Our EOF analyses showed that, globally, ENSO is the single largest cause for the extreme precipitation events. The ENSO EOF accounts for about 15%–20% of the global variance of extreme precipitation fields depending on the seasons. In some ENSO-active regions such as Australia, Indonesia, and the southern United States, the contribution is considerably higher than 20%.

The central United States experienced severe droughts during the spring–summer in 1988 (Janowiak 1988; Ropelewski 1988) and record-breaking floods in the summer of 1993 (Halpert and Smith 1995; Kunkel et al. 1995). We examined the precipitation time series of the period 1990–93 (the data for 1989–93 are from *the Monthly Climatological Data of the World*) over several regions (Table 1). We found that droughts comparable to the 1988 U.S. drought [in terms of the areal average of normalized precipitation anomalies during several consecutive months (Dai 1996)] had occurred two times (1934 and 1936) previously in the central United States and several times in all the examined regions during the period 1900–93. Severe floods comparable to the 1993 U.S. floods have been seen two times in eastern Australia and southern Africa. Table 1 also shows that severe droughts occurred more frequently in the first half of the century than thereafter in the central United States and central Europe. This suggests that as the mean precipitation has increased over northern mid- to high latitudes (cf. Fig. 8) during the last 4–5 decades, severe droughts have tended to occur less frequently in the region. When compared with ENSO indices (cf. Fig. 9), many of the severe droughts and floods are associated with ENSO events, although the most severe ones do not necessarily occur with the strongest ENSOs.

9. Summary

Monthly precipitation records from ~5300 stations were analyzed with primary focus on the period of 1900–88. A technique that combines principal component analysis and the Mann–Kendall rank sum test was developed to detect and correct stepwise instrumental discontinuities in station time series of precipitation. An assessment of Eischeid et al.'s (1991) global dataset suggests that instrumental discontinuities are unlikely to be a significant component of variation of monthly precipitation time series at most of the stations, although a small number (≈3%) of the stations, mostly

TABLE 1. The number and occurring year of severe droughts and floods that are comparable to the central U.S. 1988 drought and the 1993 floods over various regions during the period 1900–93.

Region	Severe droughts		Severe floods	
	Number	Year	Number	Year
Central United States 34°–44°N, 84°–104°W	3	1934, 1936, 1988	1	1993
Central Europe 38°–57°N, 2°W–28°E	4	1904, 1921, 1929, 1948–49	0	
Southeast China 22°–37°N, 107°–122°E	4	1917–18, 1963	0	
India 8°–28°N, 74°–88°E	2	1909–10, 1968–69	0	
Eastern Australia 40°S–5°N, 135°–160°E	9	1902, 1914, 1919, 1925–26, 1946, 1973, 1977, 1982–83, 1991–92	2	1972–73, 1975–76
Southern Africa 18°–36°S, 17°–36°E	3	1972, 1972–73, 1982–83	3	1917–18, 1924–25, 1976

in northern mid- to high latitudes, appear to have major discontinuities. The removal of the discontinuities only induces slight changes in area-averaged precipitation anomalies of large regions (mainly in northern mid- to high latitudes). On the other hand, gross screening that eliminates outliers using a single criterion less than five standard deviations can considerably underestimate area-averaged precipitation because of the skewness of precipitation histograms and can create noticeable spurious long-term changes in global and hemispheric precipitation due to the dependence of the bias on station coverage.

The spatial sampling error for the gridded precipitation anomalies is large (up to ~45%) for areas having only a few stations per 2.5° × 2.5° grid box. In the well-sampled regions such as the United States, southern Canada, Europe, eastern Australia, the Sahel, and southern Africa, the sampling error is around 10%–15%. Thus signals in precipitation fields covering only a few 2.5° × 2.5° grid boxes are generally not meaningful, especially in sparsely covered areas such as those of deserts and tropical rain forests.

In general, global annual and seasonal precipitation was relatively stable or increased slightly from 1900 to the early 1940s. It then increased sharply from the mid-1940s to the mid-1950s over global land and coastal areas and has stayed relatively high since then over most of the land areas except the Tropics, where land precipitation decreased to below the 1900–88 mean in the 1970s and 1980s. There has also been a general decreasing trend in all seasonal and annual precipitation since the late 1970s over all latitudes south of 60°N. The decadal patterns are generally consistent with those found in previous analyses of large-scale precipitation (Bradley et al. 1987; Diaz et a1. 1989; Vinnikov et al. 1990).

EOF analyses of the gridded precipitation dataset suggest that the first leading mode (~6.3% variance) in global precipitation fields is ENSO related. While the mode varies mainly on multiyear timescales and concentrates mostly in the low latitudes, it also contains decadal variability and suggests that precipitation of some midlatitude regions (namely western Canada, central western Europe, and central Eurasia) is moderately affected by ENSO. The ENSO signal is strongest in SON and weakest in JJA for global precipitation, but the seasonality is region dependent. The ENSO EOFs may be utilized in forecasting ENSO-associated precipitation anomalies around the world.

The second leading EOF depicts a linear increasing trend (~2.4 mm decade^{-1}) in global precipitation fields during the period 1900–88. The secular trend concentrates mostly in North America, mid-to high-latitude Eurasia, Argentina, and Australia, and becomes a weak decreasing trend in some parts of the low latitudes. The secular trend in global precipitation fields may be related to the observed global warming during the last 100 yr or so. The spatial patterns of the trend EOFs and the observed rate of increase are generally consistent with those of the precipitation changes in increasing CO_2 GCM experiments. For example, both in general show increased precipitation at high latitudes and decreased precipitation over low-latitude land areas.

A regional EOF analysis of precipitation over North Atlantic surrounding regions uncovered two significant modes of variation. The first mode, which has considerable power at the 11-yr timescale and accounts for ~12% of the total variance of DJF precipitation, exhibits an alternating pattern in latitude over Europe (high in central Europe and low in northern Europe, the Mediterranean, and northern Africa). This mode might be related to a pattern found in surface circulation fields over the North Atlantic that also has considerable power around decadal timescales (Deser and Blackmon 1993). The second mode, which accounts for ~10% of the variance, is an NAO-related oscillation with peak power at the 7-yr timescale. During high-NAO-index winters, precipitation tends to be ~1 σ above normal in northern (>~50°N) Europe, the eastern United States, northern Africa, and the Mediterranean, while southern Europe, eastern Canada, and western Greenland likely receive below-normal precipitation. This NAO-related mode is

consistent with precipitation anomaly patterns inferred from NAO-induced atmospheric moisture convergence (Hurrell 1995).

In midlatitudes, 1 σ wet and dry events have nearly uniform statistical characteristics. On average, dry and wet months occur about once every 6–7 months in midlatitudes. In the subtropics, the mean interval between 2 adjacent wet months or 2 dry months is longer (around 1 yr). Severe wet (above 2.5 σ) and severe dry (below -1.5 σ) events occur on average about once every 50–110 and 10–30 months in northern midlatitudes, respectively. Over global land areas, the duration of the 1-σ wet and dry events seldom (probability $< 5\%$) exceeds 2 months, and over 80% of the 1-σ events last only 1 month. The duration of the severe events rarely exceeds 1 month. ENSO accounts for about 15%–20% of the global variance of the 1-σ extreme precipitation and is the single largest cause for the global extreme precipitation events. Over the United States, the wet areas have more than doubled (from $\sim$12% to $>$24%) since the 1970s, while the dry areas have decreased by a similar amount since the 1940s. The wet severity has increased by $\sim$0.3 σ, while the dry severity has dropped a comparable amount during the last 4 decades over the United States. Similar trends are also seen over Australia. In western Europe, only the dry areas and severity decreased slightly over the last 4 decades. Severe droughts comparable to the central U.S. 1988 drought have occurred three times in the United States, and 2–9 times in each of several other regions of the world during the period 1900–93 (Table 1), while severe floods comparable to the 1993 Midwest flood occurred only once in the United States, and 2–3 times in eastern Australia and southern Africa during the period.

We have been updating our dataset to include new data for the latest years. Preliminary results show that the above conclusions are still valid.

Our analyses were limited by the poor station coverage, especially in the first half of the century and the 1980s, and by the quality of the rain gauge records, as well as the analysis method. The reliability of the dataset will be improved if all available station data of precipitation, particularly for the 1970s and 1980s for which only a portion of the stations are included in available datasets, are compiled. In recent decades, satellite microwave and infrared remote sensing data are increasingly recognized as a valuable resource for estimating precipitation (cf. Janowiak and Arkin 1991; Spencer 1993; Chang et al. 1993; Huffman et al. 1995; Xie and Arkin 1996). Satellite estimates are complimentary to ground-based rain gauge records, providing data over oceans and more complete sampling over land. The flight of the first space-based rain radar in 1997 as part of the Tropical Rainfall Measuring Mission (TRMM) will further enhance our ability to estimate precipitation globally. However, the rain gauge records from meteorological stations all over the world still remain the most accurate data available for continental and island precipitation, despite numerous problems with the rain gauge measurements. The climatology of global precipitation variations that we have complied should therefore serve as a useful standard of comparison for workers attempting to extend the space-based record of precipitation both forward and backward beyond the 3-yr duration of TRMM and outside the tropical latitudes observed by the TRMM satellite.

Acknowledgments. We are grateful to the Carbon Dioxide Information Analysis Center at Oak Ridge National Laboratory for providing the precipitation station dataset. We thank James Hansen and Ronald Miller for their helpful comments on an early draft of the paper, Brian Cairns for useful discussions on the EOF method, and Jasmin John for computational assistance. We appreciate the thoughtful comments of Clara Deser and two anonymous reviewers. The research was supported by the DOE Carbon Dioxide Research Program, the NASA Biogeochemistry and Geophysics Branch, the NASA EOS-IDS Program, the NASA Tropical Rainfall Measuring Mission No. ATM-94-22631. The gridded precipitation dataset can be downloaded from the NASA GISS web site (http://www.giss.nasa. gov).

REFERENCES

Alexandersson, H., 1986: A homogeneity test applied to precipitation data. *J. Climatol.,* **6,** 661–675.

Arkin, P. A., 1979: The relationship between fractional coverage of high cloud and rainfall accumulations during GATE over the B-scale array. *Mon. Wea. Rev.,* **107,** 1382–1387.

——, and J. Janowiak, 1991: Analysis of the global distribution of precipitation. *Dyn. Atmos. Oceans,* **16,** 5–16.

Bradley, R. S., H. F. Diaz, J. K. Eischeid, P. D. Jones, P. M. Kelly, and C. M. Goodess, 1987: Precipitation fluctuation over Northern Hemisphere land areas since the mid-19th century. *Science,* **237,** 171–175.

Chang, A. T. C., L. S. Chiu, and T. T. Wilheit, 1993: Oceanic monthly rainfall derived from SSM/I. *Eos Trans. Amer. Geophys. Union,* **74,** 505–513.

Cooley, W. W., and P. R. Lohnes, 1971: *Multivariate Data Analysis.* Wiley and Sons, 364 pp.

Cotton, W. R., and R. A. Anthes, 1989: *Storm and Cloud Dynamics.* International Geophysics Series, Vol. 44, Academic Press, 883 pp.

Creutin, J. D., and C. Obled, 1982: Objective analysis and mapping techniques for rainfall fields: An objective comparison. *Water Resour. Res.,* **18,** 423–431.

Dai, A., 1996: *Global Precipitation Variability and Its Relationship with Other Climate Changes.* Ph.D. thesis, Columbia University, 303 pp.

——, and I. Y. Fung, 1993: Can climate variability contribute to the ''missing'' CO_2 sink? *Global Biogeochem. Cycles,* **7,** 599–609.

——, A. D. Del Genio, and I. Y. Fung, 1997: Clouds precipitation and temperature range. *Nature,* **386,** 665–666.

Deser, C., and M. L. Blackmon, 1993: Surface climate variations over the North Atlantic Ocean during winter: 1900–1989. *J. Climate,* **6,** 1743–1753.

Diaz, H. F., R. S. Bradley, and J. K. Eischeid, 1989: Precipitation fluctuations over global land areas since the late 1800's. *J. Geophys. Res.,* **94,** 1195–1210.

Duchon, C. E., 1979: Lanczos filtering in one and two dimensions. *J. Appl. Meteor.,* **18,** 1016–1022.

Easterling, D. R., and T. C. Peterson, 1995: A new technique for detecting and adjusting for undocumented discontinuities in climatological time series. *Int. J. Climatol.,* **15,** 369–377.
——, ——, and T. R. Karl, 1996: On the development and use of homogenized climate datasets. *J. Climate,* **9,** 1429–1434.
Eischeid, J. K., R. S. Bradley, and P. D. Jones, 1991: A comprehensive precipitation data set for global land areas. DOE Tech. Rep. TR051, DOE ER-69017T-H1, 81 pp. [Available from National Technical Information Service, U.S. Dept. of Commerce, 5285 Port Royal Road, Springfield, VA 22161.]
Elliott, W. P., M. E. Smith, and J. K. Angell, 1991: Monitoring tropospheric water vapor changes using radiosonde data. *Greenhouse-Gas-Induced Climate Change: A Critical Appraisal of Simulations and Observations,* M. E. Schlessinger, Ed., Elsevier, 311–328.
Følland, C. K., T. R. Karl, and K. Y. Vinnikov, 1990: Observed climate variations and change. *Climate Change, The IPCC Scientific Assessment,* J. T. Houghton, G. J. Jenkins, and J. J. Ephraums, Eds., Cambridge University Press, 201–238.
——, ——, N. Nicholls, B. S. Nyenzi, D. E. Parker, and K. Y. Vinnikov, 1992: Observed climate variability and change. *Climate Change 1992, The Supplementary Report to The IPCC Scientific Assessment,* J. T. Houghton, B. A. Callander, and S. K. Varney, Eds., Cambridge University Press, 135–170.
Gaffen, D. J., T. P. Barnett, and W. P. Elliott, 1991: Space and time scales of global tropospheric moisture. *J. Climate,* **4,** 989–1008.
——, W. P. Elliott, and A. Robock, 1992: Relationship between tropospheric water vapor and surface temperature as observed by radiosondes. *Geophys. Res. Lett.,* **19,** 1839–1842.
Greenwald, T. J., G. L. Stephens, T. H. Vonder Harr, and D. L. Jackson, 1993: A physical retrieval of cloud liquid water over the global oceans using Special Sensor Microwave/Imager (SSM/I) observations. *J. Geophys. Res.,* **98,** 18 471–18 488.
Groisman, P. Y., and D. R. Easterling, 1994: Variability and trends of total precipitation and snowfall over the United States and Canada. *J. Climate,* **7,** 184–205.
——, and D. R. Legates, 1994: The accuracy of United States precipitation data. *Bull. Amer. Meteor. Soc.,* **75,** 215–227.
——, V. V. Koknaeva, T. A. Belokrylova, and T. R. Karl, 1991: Overcoming biases of precipitation measurement: A history of the USSR experience. *Bull. Amer. Meteor. Soc.,* **72,** 1725–1733.
Halpert, M. S., and T. M. Smith, 1994: Seasonal climate summary: The global climate for March–May 1993: Mature ENSO conditions persist and a blizzard blankets the eastern United States. *J. Climate,* **7,** 1772–1793.
Hansen, J., and S. Lebedeff, 1987: Global trends of measured surface air temperature. *J. Geophys. Res.,* **92,** 13 345–13 372.
——, and ——, 1988: Global surface air temperatures: Update through 1987. *Geophys. Res. Lett.,* **15,** 323–326.
Henderson-Sellers, A., 1992: Continental cloudiness changes this century. *Geo J.,* **27,** 255–262.
Huffman, G. J., R. F. Adler, B. Rudolf, U. Scheider, and P. R. Keehn, 1995: Global precipitation estimates based on a technique for combining satellite-based estimates, rain gauge analysis, and NWP model precipitation information. *J. Climate,* **8,** 1284–1295.
Hulme, M., 1992: A 1951–80 global land precipitation climatology for the evaluation of general circulation models. *Climate Dyn.,* **7,** 57–72.
Hurrell, J. W., 1995: Decadal trends in the North Atlantic oscillation: Regional temperature and precipitation. *Science,* **269,** 676–679.
IPCC, 1990: *Climate Change, The IPCC Scientific Assessment.* J. T. Houghton, G. J. Jenkins, and J. J. Ephraums, Eds., Cambridge University Press, 364 pp.
——, 1992: *Climate Change 1992: The Supplementary Report to the IPCC Scientific Assessment.* J. T. Houghton, B. A. Callander, and S. K. Varney, Eds., Cambridge University Press, 200 pp.
——, 1996: *Climate Change 1995, The Science of Climate Change.* J. T. Houghton, L. G. Meira Filho, B. A. Callander, N. Harris, A. Katternberg, and K. Maskell, Eds., Cambridge University Press.
Jaeger, L., 1983: Monthly and areal patterns of mean global precipitation. *Variation in the Global Water Budget,* A. Street-Perot and Coeditors, D. Reidel Publishing, 129–140.
Janowiak, J. E., 1988: Seasonal climate summary: The global climate for March–May 1988: The end of the 1986–87 Pacific warm episode and the onset of widespread of drought in the United States. *J. Climate,* **1,** 1019–1040.
——, and P. A. Arkin, 1991: Rainfall variations in the Tropics during 1986–1989, as estimated from observations of cloud-top temperature. *J. Geophys. Res.,* **96,** 3359–3373.
Jones, P. D., and K. R. Briffa, 1992: Global surface air temperature variations over the twentieth century: Part I, spatial, temporal and seasonal details. *Holocene,* **2,** 165–179.
Karl, T. R., and P. M. Steurer, 1990: Increased cloudiness in the United States during the first half of the twentieth century: Fact or fiction? *Geophys. Res. Lett.,* **17,** 1925–1928.
——, R. G. Quayle, and P. Y. Groisman, 1993: Detecting climate variations and changes: New challenges for observing and data management systems. *J. Climate,* **6,** 1481–1494.
Kendall, M. G., 1970: *Rank Correlation Methods,* Griffin, 202 pp.
Kunkel, K. E., S. A. Changnon, and J. R. Angel, 1995: Climatic aspects of the 1993 upper Mississippi River basin flood. *Bull. Amer. Meteor. Soc.,* **76,** 811–822.
Kutzbach, J. E., 1967: Empirical eigenvectors of sea-level pressure, surface temperature and precipitation complexes over North America. *J. Appl. Meteor.,* **6,** 791–802.
Lamb, P. J., and A. Peppler, 1992: Further case studies of tropical Atlantic surface atmospheric and oceanic patterns associated with sub-Saharan drought. *J. Climate,* **5,** 476–488.
Lau, K.-M., and P. J. Sheu, 1988: Annual cycle, quasi-biennial oscillation, and Southern Oscillation in global precipitation. *J. Geophys. Res.,* **93,** 10 975–10 988.
Lebel, T., G. Bastin, C. Obled, and J. D. Creutin, 1987: On the accuracy of areal rainfall estimation: A case study. *Water Resour. Res.,* **23,** 2123–2134.
Legates, D. R., and C. J. Willmott, 1990: Mean seasonal and spatial variability in gauge-corrected, global precipitation. *Int. J. Climatol.,* **10,** 111–127.
Manabe, S., M. D. Spelman, and R. J. Stouffer, 1992: Transient response of a coupled ocean–atmosphere model to gradual changes of atmospheric CO_2. Part II: Seasonal response. *J. Climate,* **5,** 105–126.
Mann, H. B., 1945: Non-parametric test of randomness against trend. *Econometrica,* **13,** 245–259.
Mendenhall, W., D. D. Wackerly, and R. L. Scheaffer, 1990: *Mathematical Statistics with Applications.* 4th ed. PWS-KENT Publishing, 818 pp.
Namias, J., 1983: Some causes of United States drought. *J. Climate Appl. Meteor.,* **22,** 30–39.
Nicholls, N., and B. Lavery, 1992: Australian rainfall trends during the twentieth century. *Int. J. Climatol.,* **12,** 153–163.
Nicholson, S. E., 1993: An overview of African rainfall fluctuations of the last decade. *J. Climate,* **6,** 1463–1466.
North, G. R., T. L. Bell, and R. F. Cahalan, 1982: Sampling errors in the estimation of empirical orthogonal functions. *Mon. Wea. Rev.,* **110,** 699–706.
Rasmusson, E. M., and T. H. Carpenter, 1982: Variations in tropical sea surface temperature and surface wind fields associated with the Southern Oscillation/El Niño. *Mon. Wea. Rev.,* **110,** 354–384.
Richards, F., and P. A. Arkin, 1981: On the relationship between satellite-observed cloud cover and precipitation. *Mon. Wea. Rev.,* **109,** 1081–1093.
Ropelewski, C. F., 1988: The global climate for June–August 1988: A swing to the positive phase of the Southern Oscillation, drought in the United States, and abundant rain in monsoon areas. *J. Climate,* **1,** 1153–1174.
——, and M. S. Halpert, 1987: Global and regional scale precipitation patterns associated with the El Niño/Southern Oscillation. *Mon. Wea. Rev.,* **115,** 1606–1626.

——, and ——, 1989: Precipitation patterns associated with the high-index phase of the Southern Oscillation. *J. Climate*, **2,** 268–284.

Ross, R. J., and W. P. Elliott, 1996: Tropospheric water vapor climatology and trends over North America: 1973–93. *J. Climate*, **9,** 3561–3574.

Russell, G. L., J. R. Miller, and D. Rind, 1995: A coupled atmosphere–ocean model for transient climate change studies. *Atmos.–Ocean*, **33,** 687–730.

Sevruk, B., 1982: Methods of correcting for systematic error in point precipitation measurement for operational use. Operational Hydrology Rep. 21, WMO 589, 91 pp.

——, 1993: Systematic error of precipitation measurements. *Global Energy and Water Cycle Experiment (GEWEX) News*, **3,** 4–5.

Shea, D. J., 1986: Climatological atlas: 1950–1979. NCAR Tech. Note NCAR TN-269+STR, 35 pp. [Available from National Center for Atmospheric Research, Boulder, CO 80307.]

Spencer, R. W., 1993: Global oceanic precipitation from the MSU during 1979–91 and comparisons to other climatologies. *J. Climate*, **6,** 1301–1326.

Trenberth, K. E., and G. W. Branstator, 1992: Issues in establishing causes of the 1988 drought over North America. *J. Climate*, **5,** 159–173.

——, and C. J. Guillemot, 1996: Physical processes involved in the 1988 drought and 1993 floods in North America. *J. Climate*, **9,** 1288–1298.

Vinnikov, K. Y., P. Y. Groisman, and K. M. Lugina, 1990: Empirical data on contemporary global climate changes (temperature and precipitation). *J. Climate*, **3,** 662–677.

Vose, R. S., R. Heim, R. L. Schmoyer, T. R. Karl, P. M. Steurer, J. K. Eischeid, and T. C. Peterson, 1992: The global historical climatology network: Long-term monthly temperature, precipitation, sea level pressure, and station pressure data. ORNL/CDIAC-53, NDP-041, Carbon Dioxide Information Analysis Center, Oak Ridge National Laboratory, Oak Ridge, TN. [Available from National Technical Information Service, U.S. Dept. of Commerce, 5285 Port Royal Road, Springfield, VA 22161.]

Wallace, J. M., and D. S. Gutzler, 1981: Teleconnections in the geopotential height field during the Northern Hemisphere winter. *Mon. Wea. Rev.*, **109,** 784–812.

——, Y. Zhang, and K.-H. Lau, 1993: Structure and seasonality of interannual and interdecadal variability of the geopotential height and temperature fields in the Northern Hemisphere troposphere. *J. Climate*, **6,** 2063–2082.

——, ——, and L. Bajuk, 1996: Interpretation of interdecadal trends in Northern Hemisphere surface air temperature. *J. Climate*, **9,** 249–259.

Washington, W. M., and G. A. Meehl, 1989: Climate sensitivity due to increased CO_2: Experiments with a coupled atmosphere and ocean general circulation model. *Climate Dyn.*, **4,** 1–38.

WMO, 1989: Proceedings of international workshop on precipitation measurements. WMO Instruments and Observing Methods Rep. 48, WMO/TD-328, World Meteorological Organization, Geneva, Switzerland, 584 pp.

Wright, P. B., 1984: Relationship between indices of the Southern Oscillation. *Mon. Wea. Rev.*, **112,** 1913–1919.

Xie, P. P., and P. A. Arkin, 1995: An intercomparison of gauge observations and satellite estimates of monthly precipitation. *J. Appl. Meteor.*, **34,** 1143–1160.

——, and ——, 1996: Analysis of global monthly precipitation using gauge observations, satellite estimates, and numerical model predictions. *J. Climate*, **9,** 840–858.